Journal of the Mechanics and Physics of Solids 89 (2016) 1–15

Contents lists available at ScienceDirect

Journal of the Mechanics and Physics of Solids

journal homepage: www.elsevier.com/locate/jmps

Mechanical annealing under low-amplitude cyclic loading in micropillars

Yi-nan Cui [a], Zhan-li Liu [a,*], Zhang-jie Wang [b], Zhuo Zhuang [a,*]

[a] Applied Mechanics Lab., School of Aerospace Engineering, Tsinghua University, Beijing 100084 China
[b] Center for Advancing Materials Performance from the Nanoscale (CAMP-Nano) & Hysitron Applied Research Center in China (HARCC), State Key Laboratory for Mechanical Behavior of Materials, Xi'an Jiaotong University, Xi'an 710049, China

ARTICLE INFO

Article history:
Received 27 March 2015
Received in revised form
22 December 2015
Accepted 20 January 2016
Available online 21 January 2016

Keywords:
Submicron scale
Single crystal plasticity
Dislocation annihilation
Junction stability
Cyclic irreversibility

ABSTRACT

Mechanical annealing has been demonstrated to be an effective method for decreasing the overall dislocation density in submicron single crystal. However, simultaneously significant shape change always unexpectedly happens under extremely high monotonic loading to drive the pre-existing dislocations out of the free surfaces. In the present work, through in situ TEM experiments it is found that cyclic loading with low stress amplitude can drive most dislocations out of the submicron sample with virtually little change of the shape. The underlying dislocation mechanism is revealed by carrying out discrete dislocation dynamic (DDD) simulations. The simulation results indicate that the dislocation density decreases within cycles, while the accumulated plastic strain is small. By comparing the evolution of dislocation junction under monotonic, cyclic and relaxation deformation, the cumulative irreversible slip is found to be the key factor of promoting junction destruction and dislocation annihilation at free surface under low-amplitude cyclic loading condition. By introducing this mechanics into dislocation density evolution equations, the critical conditions for mechanical annealing under cyclic and monotonic loadings are discussed. Low-amplitude cyclic loading which strengthens the single crystal without seriously disturbing the structure has the potential applications in the manufacture of defect-free nano-devices.

1. Introduction

Reducing the dislocation density at the submicron scale is important for obtaining multifunctional micro-devices, such as high-strength (Bei et al., 2008), improved dielectric properties (Alpay et al., 2004) and electrical and thermal conductivities (Watling and Paul, 2011). There is a considerable body of evidences that dislocation density tends to decrease in small submicron single crystal when subjected to monotonic loading (Greer and Nix, 2006; Shan et al., 2008; Uchic et al., 2009). This process named as "mechanical annealing" (Shan et al., 2008) is usually attributed to the massive dislocation escape from free surface (Greer, 2006; Greer and Nix, 2006; Wang et al., 2012). Generally, the occurrence of this phenomenon depends on the sample size (several hundred nanometers) and applied stress level (several GPa). Smaller sample size corresponds to higher attractive image force and more significant surface annihilation, while higher stress means that more dislocation junctions can be broken. However, the relative high applied monotonic loading (as high as several GPa) also

* Corresponding authors.
E-mail addresses: liuzhanli@tsinghua.edu.cn (Z.-l. Liu), zhuangz@tsinghua.edu.cn (Z. Zhuang).

http://dx.doi.org/10.1016/j.jmps.2016.01.011
0022-5096/

triggers a significant amount of dislocation multiplication. The decreasing of dislocation density requires the annihilation of both the pre-existing and the multiplied dislocations. This leads to evident changes of the specimen shape, which is not anticipated in the practical applications. So it will be very attractive if there exists a new loading method (e.g., with relative low-amplitude) to drive out the dislocations and at the same time keep the specimen shape without significant change.

This raises the question whether the non-monotonic loading performed with relative low-amplitude can disengage the complex pre-existing dislocation structures without causing significant dislocation multiplication. Generally, under cyclic loading condition, dislocation accumulation by forming pattern structures such as well-ordered veins and walls (Aifantis, 1987), is usually expected even at the micron scale (Zhang et al., 2006). Whether the defect healing can be observed if the external size further decreases to several hundred nanometers? A convenient way to verify the aforementioned idea is to adopt in-situ TEM experiment and three-dimensional discrete dislocation dynamic (3D-DDD) simulation method. 3D-DDD has been proved to be an effective method to reveal the dynamic evolution of dislocations in small crystals (Csikor et al., 2007; Devincre et al., 2008; El-Awady, 2015; El-Awady et al., 2009; Groh and Zbib, 2009). In the current work, the cyclic loading tests with relative low-peak stress are carried out by both experiments and 3D-DDD simulations on Al micro-pillar with the diameter of a few hundred nanometers. It is somewhat surprising to observe that the initial high dislocation density significantly decreases within cycles. Particularly noteworthy is that there is no such pronounced shape change compared with relative high stress monotonic loading. This phenomenon makes it exhibit great promise for applications in obtaining high-strength crystal with low density dislocations.

Naturally this intriguing observation raises several questions to us. Firstly, how could the low cyclic stress contribute to the decline of dislocation density? How will cyclic loading affect the dislocation annihilation and multiplication process? In addition, both the line tension model (Dupuy and Fivel, 2002) and atomic level analysis (Rodney and Phillips, 1999) indicate that the failure of dislocation junction often requires high enough applied stress. How can dislocation junctions be destroyed without high-stress under cyclic loading? Previous studies mainly focus on the stability of dislocation junction under monotonic loading (Dupuy and Fivel, 2002; Picu and Soare, 2010). Little attention is paid on the cyclic stability of dislocation

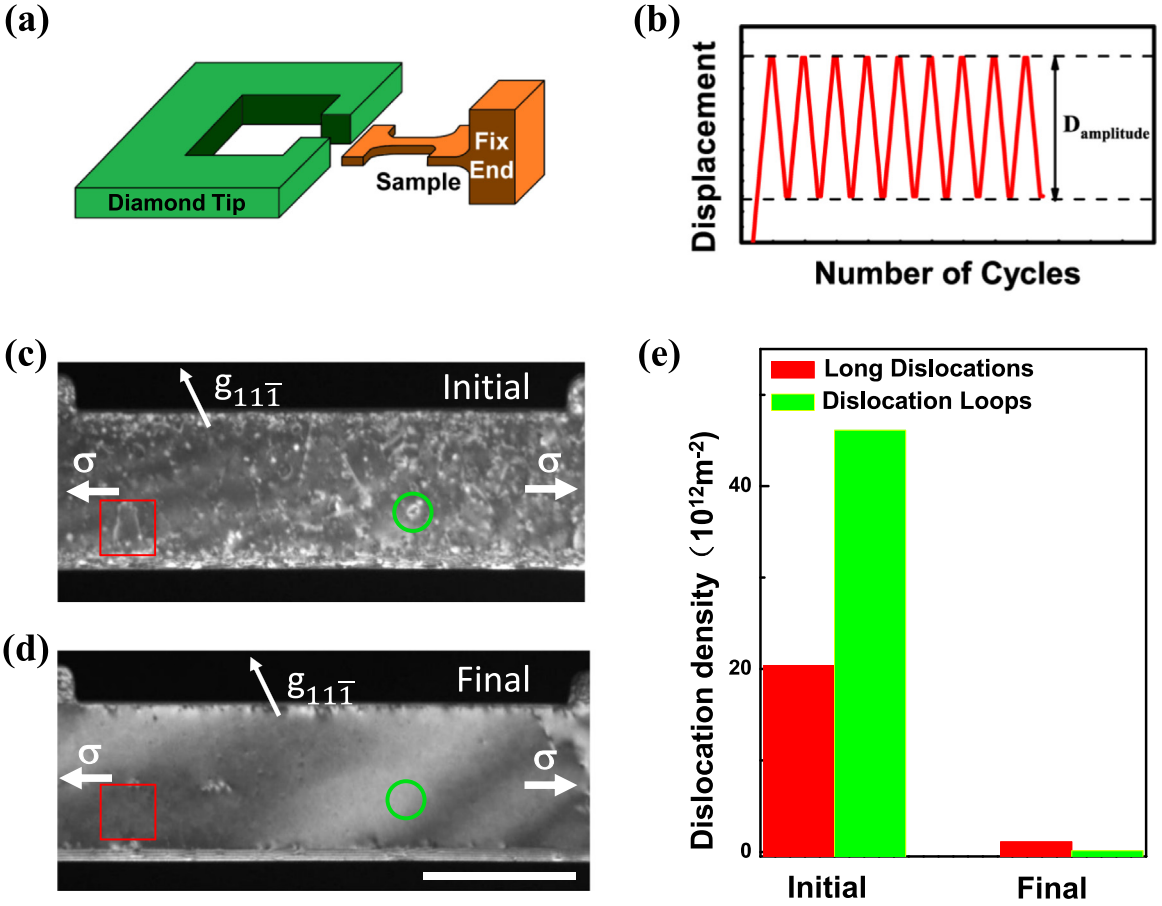

Fig. 1. A typical example of mechanical annealing of defected Al single crystal through low-amplitude cyclic straining. (a) Schematic of in situ cyclic tension loading test inside a TEM. (b) Cyclic loading displacement program. (c) Dark-field TEM image of as-fabricated Al single crystal. (d) Dark-field TEM image of Al single crystal after mechanical annealing. (e) The densities of the two types of dislocations before and after mechanical annealing. The scale bar in (d) represents 500 nm (Wang et al., 2015). (For interpretation of the references to color in this figure legend, the reader is referred to the web version of this article.)

Table 1
Cyclic loading parameters for Al sample, where "–" represents that the value is too small to be measured.

	Group1	Group2	Group3	Group4	Group5	Group6
Cycle number	80	175	80	65	300	1
ε_{max}	–	–	–	–	0.004 ± 0.002	0.006 ± 0.002
ε_{min}	–	–	–	–	–	–
σ_{max} (MPa)	38	44	170	90	250	420
σ_{min} (MPa)	12	−23	16	0	−92	14

junctions. Secondly, how to predict the dislocation density evolution under low cyclic stress? Under monotonic loading, Greer (2006) firstly proposed a dislocation surface annihilation model to predict the dislocation density evolution. This model is improved by Zhou et al. (2011) to consider the loading orientation effect and further improved by Cui et al. (2014) to incorporate a single arm dislocation source mechanism. Then, how to extend this model to apply to cyclic deformation remains to be explored. At last, determining the critical conditions for mechanical annealing is also of special interest. Since both monotonic and cyclic loadings can contribute to dislocation annihilation, a comparison can be made from aspects of the critical size, to discuss the occurrence condition of dislocation starvation. Addressing these problems is important not only for deeply understanding crystal plasticity at submicron scale, but also for engineering application.

This paper is aimed at systematically resolving these questions and clarifying the underlying mechanism under low-amplitude cyclic loading condition. It is organized as follows: Section 2 presents the experimental results for the low-amplitude cyclic tests of Al pillar. Section 3 gives 3D-DDD simulation results to present the characteristic dislocation behavior and discuss junction stability under low-stress cyclic deformations. The underlying dislocation mechanism is discussed in Section 4. Then, by considering the influence of recoverable multiplication and dislocation annihilation enhanced by irreversible slip, the critical conditions of mechanical annealing are discussed in Section 5. Finally, the paper ends with some concluding remarks given in Section 6.

2. Experiments

In situ low-amplitude cyclic loading experiments are carried out for pure single crystalline Al pillar inside a TEM (Wang et al., 2015). The experimental setup is schematically indicated in Fig. 1a and b. Displacement rate controlled small amplitude cyclic loading is applied along $[\bar{1}11]$ direction with a frequency of $1/2.2\ s^{-1}$. As described in Table 1, six groups of cyclic loadings are applied. The sample is fabricated by focused ion beam (FIB). The nominal dimensions of cuboid-shaped sample are 300 nm in thickness and 500 nm in width.

Fig. 1c gives the dark-field image of the as-fabricated sample with beam direction close to [110] zone axis. There are large populations of long line-like dislocations (one example marked by red rectangle in Fig. 1c) and dislocation loops induced by ion beam milling (one example marked by green circle in Fig. 1c). However, most of these defects are driven out of the crystal after multiple sets of low-amplitude cyclic stress, as shown in Fig. 1d. This is also verified by using other reflection vectors. Quantitatively speaking, the peak engineering stress value is smaller than 250 MPa during the first five groups according to Table 1. The density of long dislocation line and dislocation loop markedly changes from $20 \times 10^{12}\ m^{-2}$ to $4.1 \times 10^{12}\ m^{-2}$ and from $46 \times 10^{12}\ m^{-2}$ to $0.13 \times 10^{12}\ m^{-2}$, respectively during the first five groups of cyclic loading, and further decreases to $1.1 \times 10^{12}\ m^{-2}$ and $0.13 \times 10^{12}\ m^{-2}$ (see Fig. 1e), respectively after the last group of cyclic loading in Table 1.

Importantly, the shape of sample is also found little changed. The total plastic strain measured between the two markers is only $0.2 \pm 0.1\%$. In addition, the yield strength after such cyclic loading is significantly improved as expected. More details of the experimental procedure and results are given in the paper by Wang et al. (2015).

These results demonstrate that mechanical annealing by low-amplitude cyclic loading can be achieved experimentally. It points to a versatile engineering pathway for controlled defect engineering in submicrometer-sized metal crystals, thereby obviating the need for thermal annealing or significant plastic deformation that could cause change in shape and/or dimensions of the specimen. However, the underlying dynamic mechanism still needs to be further revealed by 3D-DDD simulation. In the following, 3D-DDD simulation is adopted to unveil the characteristic dislocation behavior and physical origin of breakdown of the pinned dislocation under the repeated low-amplitude straining.

3. Simulations

Several sets of 3D-DDD simulations are carried out under different loading conditions to systematically explore the dislocation behavior. In the simulation, an arbitrary curve dislocation is discretized into several straight dislocation segments. Dislocation motion is considered to be in the over-damped regime, the velocity of each dislocation segment is determined by the total force acting on it divided by the viscous drag coefficient. The total force contains the Peach–Koehler (PK) force induced by external loading and all other defects, line tension force, as well as image force due to free surface (Liu

et al., 2009). Several factors are taken into account in the simulations, such as free surface truncation effect, collinear interaction, the formation and destruction of dislocation locks. Recently, Hussein et al. (2015) proposed a complete model to consider different kinds of cross slip. Here, for simplicity, thermal activated cross slip effect is considered by introducing a probability parameter of cross slip event using Monte-Carlo method (Devincre, 1996; Kubin et al., 1992), which is also widely used by the previous researchers. More details of the current 3D-DDD method can be found in our previous papers (Cui et al., 2014, 2015a, 2015b; Gao et al., 2010; Liu et al., 2009).

Similar to experiments, 3D-DDD simulations are conducted in cuboid-shaped pillar. The single crystal material is also taken to be Al, with shear modulus $\mu=27$ GPa, Poisson's ratio $\nu=0.347$ and viscous drag coefficient $B=10^{-4}$ Pa s (Motz et al., 2008). The top surface of a pillar uniformly undergoes a strain controlled loading along [001] crystal orientation via a cut-off plastic strain rate method. For each time increment $dt=10^{-12}$ s^{-1}, if the calculated plastic strain rate $\dot{\varepsilon}^{p}$ is lower than the applied strain rate $\dot{\varepsilon}$, the total strain increases by an increment $\dot{\varepsilon}\cdot dt$; otherwise, the total strain is not increased in this step. This means after an external displacement is applied, the fully relaxed dislocation configuration requires to be reached after multiple time increment steps. Here, $\dot{\varepsilon}$ is set to 2400 s^{-1}, which is found to compromise between minimizing strain rate artifacts and rationalizing computational time. The loading method that uses the plastic strain rate as a criterion to increase load is commonly used in the other DDD simulations (Lee et al., 2013; Rao et al., 2008; Zhou et al., 2011), which can make the plastic strain sufficiently release and get stable at the relaxed dislocation configuration. Besides, the obtained stress–strain response is relatively strain-rate insensitive for the considered sample size as indicated by previous studies (Espinosa et al., 2006; Lee et al., 2013).

3.1. Cyclic behavior of collective dislocations

The micropillar with relatively high initial dislocation density is investigated here, which is similar to the situation in the experiments. Firstly, the straight dislocation lines randomly spread on all of twelve slip systems for FCC. Before applying load, the pillars are stress-relaxed to reach an energy equilibrium state. An example is shown in Fig. 2. The dislocation junctions emerge as a natural outcome of dislocation interaction, without the requirement of putting initial fixed pinning points. The obtained initial dislocation density is within the range of experimentally measured dislocation density for FIB fabricated micropillar (10^{13}~10^{14}m^{-2}). Two kinds of small strain cyclic loadings are imposed on the top of pillar with the maximum strain ε_{max} twice the minimum one ε_{min}. In the one case, $\varepsilon_{max}=2\varepsilon_{min}=0.1\%$, and in the other case, $\varepsilon_{max}=2\varepsilon_{min}=0.2\%$. The corresponding peak stress is lower than 140 MPa, which is even lower than the yield stress $\sigma_y>200$ MPa for Al micropillar with diameter 400 nm.

As revealed in Fig. 3a, the dislocation density decreases within cycles for micropillar with cross-section 400×400 nm and height 800 nm, which is consistent with the experimental sample. During a loading stage of the first cycle, the dislocation annihilation rate almost exhibits a linear relation with the applied strain. Thus, the higher the peak strain is, the lower the dislocation density is after the first cycle. Actually, this corresponds to the dislocation density evolution trend during the initial microplastic stage of monotonic loading (Motz et al., 2009). Comparing the initial stable dislocation structure in Fig. 2 and the green dislocation configuration in Fig. 3b, the decrease of dislocation density under very low-amplitude cyclic strains is mainly induced by the surface annihilation of mobile dislocations during the first several cycles. The comparison of dislocation configuration in Figs. 2 and 3c shows that in the case of larger peak strain, the broken of weak dislocation junctions also contributes to the decrease of dislocation density.

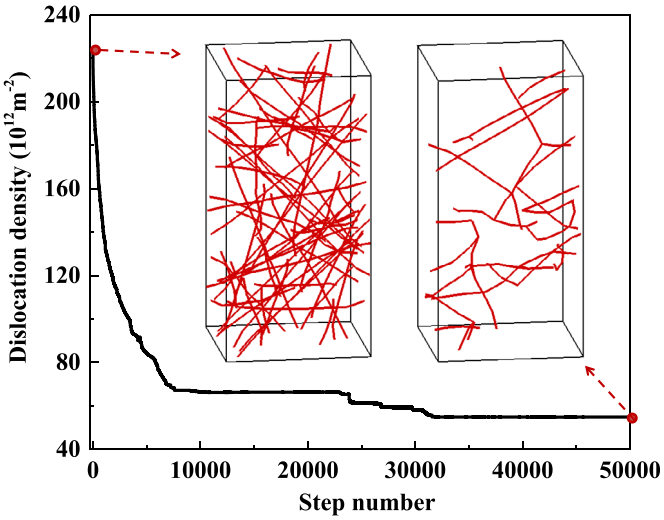

Fig. 2. Evolution of dislocation density during stress-relaxation process for micropillar with diameter 400 nm, the insets show the corresponding dislocation snapshots before and after stress relaxation.

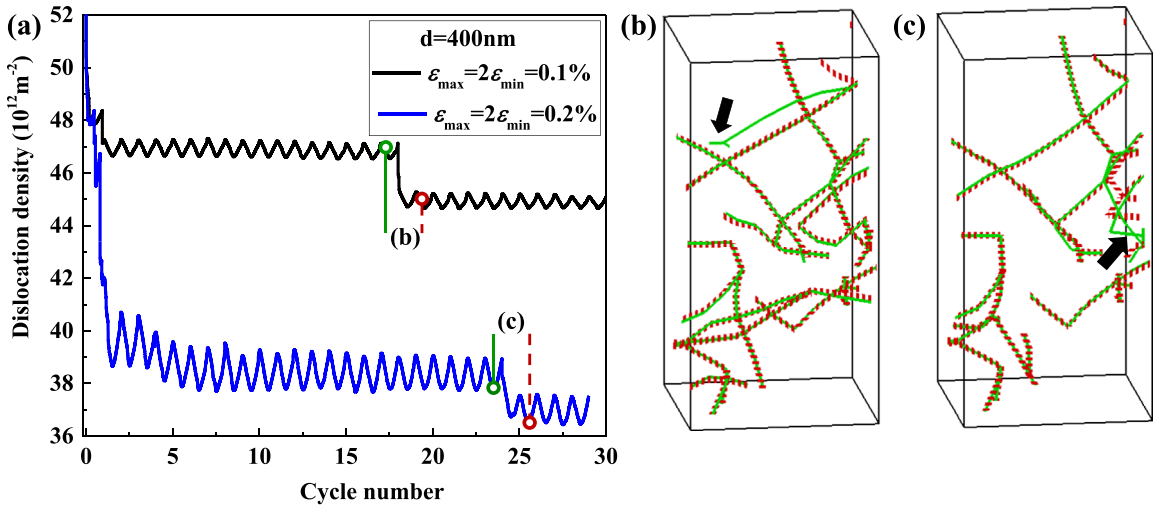

Fig. 3. (a) Evolution of dislocation density during low-amplitude cyclic loading for micropillar with diameter 400 nm; (b and c) snapshots of dislocation configuration corresponding to the same color marked circles in (a). The arrows indicate the junctions that are destroyed during cyclic loading. (For interpretation of the references to color in this figure legend, the reader is referred to the web version of this article.)

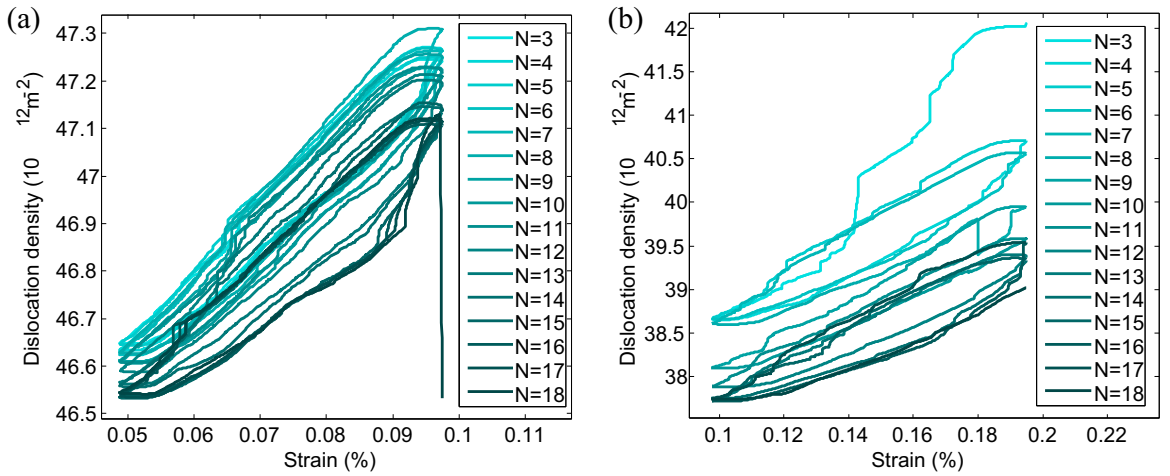

Fig. 4. Evolution of dislocation density for micropillar with diameter 400 nm during the first several cycles under (a) $\varepsilon_{max}=2\varepsilon_{min}=0.1\%$ and (b) $\varepsilon_{max}=2\varepsilon_{min}=0.2\%$.

From Fig. 3a, the dislocation density seems to change little from cycle number $N=3$ to $N=18$, especially for the loading condition $\varepsilon_{max}=2\varepsilon_{min}=0.1\%$. This is because the dislocations, which are very easy to annihilate under the current stress level, are gradually exhausted during the first two cycles. In such small sample, the characteristic length of dislocation source is short, which means high activation stress for these sources. Thus, the low applied stress is not high enough to trigger dislocation source operation, and no substantial dislocation multiplication occurs. It is observed that most of the dislocation segments bow out upon loading and shrink backward during unloading from the second cycle. This leads to a first increase and a subsequent decrease of dislocation density during each cycle (see Fig. 3a). The recovery of dislocation density during unloading is also observed in DDD simulations by Déprés et al. (2008). Note that the reverse dislocation motion does not fully recover the dislocation configuration back to that at the beginning of the cycle. In such limited size, the incomplete reverse dislocation motion provides opportunities for their annihilation at a nearby free surface, leading to a gradual decrease of dislocation density as show in Fig. 4. This exactly reflects the advantage of cyclic loading upon monotonic loading when triggering dislocation annihilation. Despite that the dislocation density only decreases a very small amount after each cycle due to the small strain amplitude, the cumulative decline with increasing number of cycles can still be very large and may ultimately lead to significant decrease of dislocation density. This phenomenon is fundamentally different from the cyclic behavior for bulk materials.

More interestingly, after multiple cycles, the dislocation junction can be broken and expelled from the crystal, leading to a sudden decline of dislocation density at some cycle. This phenomenon is presented by the green solid and red dotted

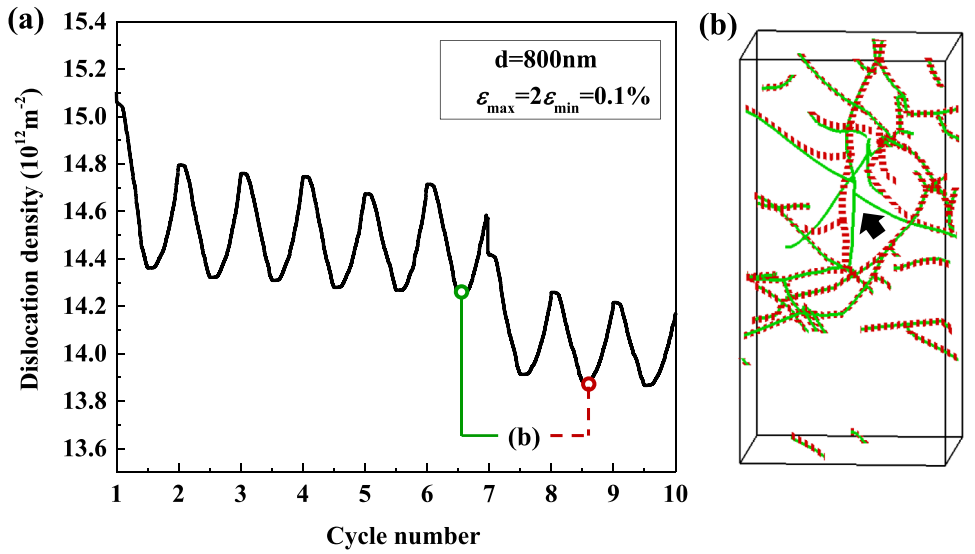

Fig. 5. (a) Evolution of dislocation density during low-amplitude cyclic loading for micropillar with diameter 800 nm; (b) snapshots of dislocation configuration corresponding to the same color marked circles in (a). The arrows indicate the junctions that are rearranged during cyclic loading. (For interpretation of the references to color in this figure legend, the reader is referred to the web version of this article.)

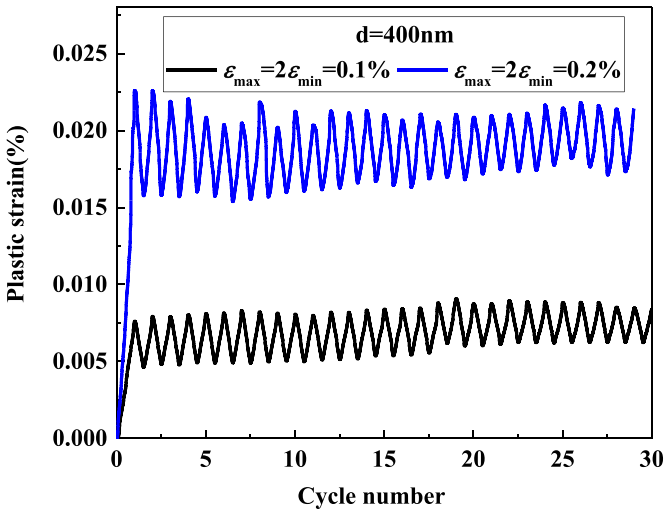

Fig. 6. Evolution of plastic strain within cycles for micropillar with diameter 400 nm.

dislocation configurations in Fig. 3b and c. Similar behavior is also observed in micropillar with cross-section 800 × 800 nm^2 and height 1600 nm under the loading condition $\varepsilon_{max}=2\varepsilon_{min}=0.1\%$ (see Fig. 5). By way of contrast, for larger sample, there is large possibility for the junction to interact with other dislocation before directly failing by annihilating from free surface. Therefore, the dislocation configuration only rearranged after the failure of some dislocation junction in large sample.

In addition, the evolution of the accumulated plastic strain in Fig. 6 illustrates that from the second cycle, the plastic strain during unloading stage is almost comparable to the plastic strain during loading stage. Rajagopalan et al. (2007) proposed that the driven force for the recoverable plastic deformation arise from residual internal stresses caused by inhomogeneous deformation. Moreover, it is noteworthy that the accumulated plastic strain after multiple cycles keeps low during the whole low cyclic loading process, which means this kind of loading mode only causes small shape change.

3.2. *Cyclic instability of dislocation junction*

The simulation results above present an interesting phenomenon that the dislocation junction can be failed under low-amplitude cyclic stress. This section is aimed at revealing its underlying mechanism. For the complex dislocation configurations, the dynamic evolution of dislocations is blurred by the difficulty in distinguishing the role of cyclic loading from collective dislocation interaction. Thus, we turn to consider a simple but illustrative case. Simulations only containing one

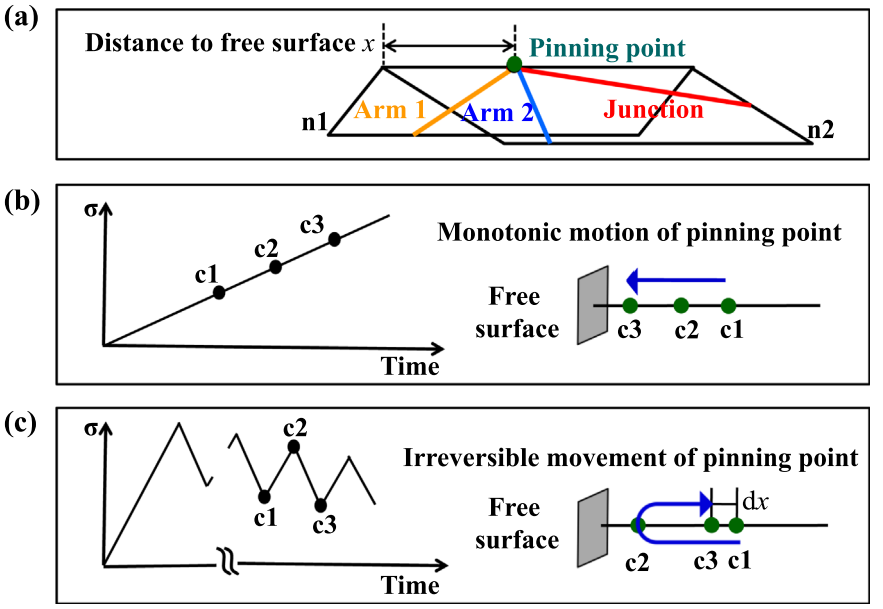

Fig. 7. (a) Schematic definition of distance of pinning points to free surface (x) for a glissile junction; schematic diagram for junction destruction process under (b) monotonic deformation and (c) small strain cyclic deformation.

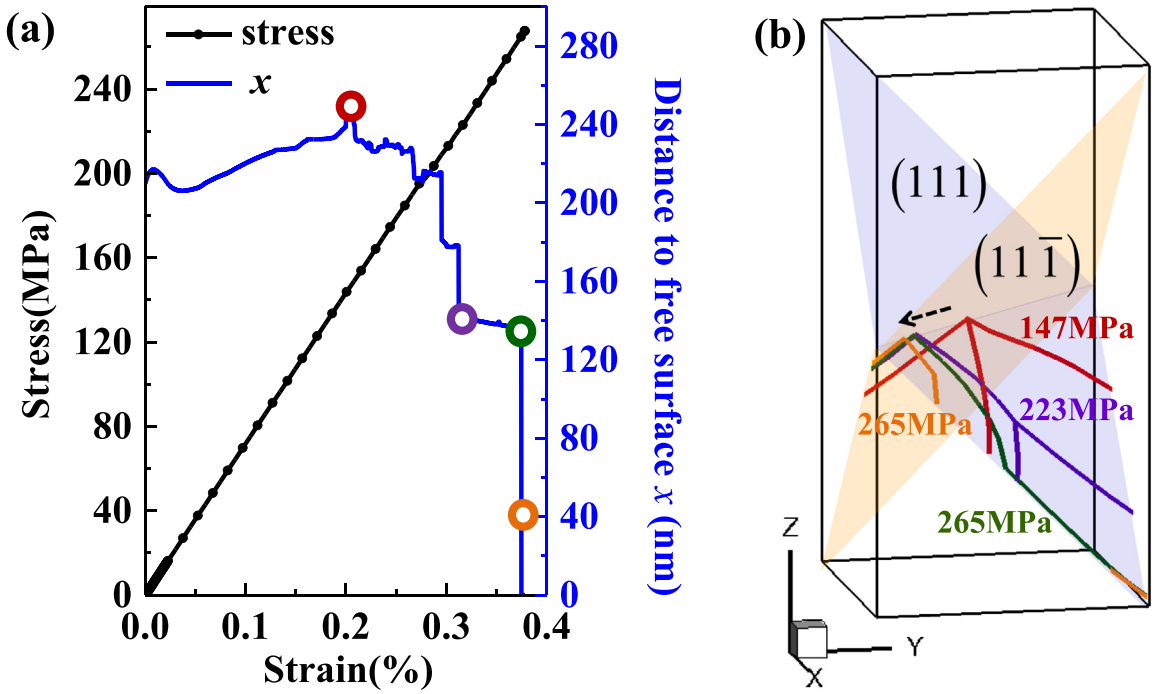

Fig. 8. (a) Evolution of stress and distance of pinning point to free surface versus applied strain under monotonic tension for a glissile junction; (b) snapshots of dislocation configuration corresponding to the same color marked circles in the curve. (For interpretation of the references to color in this figure legend, the reader is referred to the web version of this article.)

dislocation junction are carried out.

The glissile and Lomer–Cottrell (LC) junctions are widely observed in FCC crystal. They are determined as the strongest and significant junctions (Dupuy and Fivel, 2002; Franciosi and Zaoui, 1982), with representative glissile and sessile character, respectively. Thus, they are chosen to be investigated in the following sections to understand the cyclic failure mechanism of dislocation junction. By comparing with the response under monotonic loading and peak stress relaxation, the

dislocation annihilation mechanism under different loading modes is also analyzed.

3.2.1. Glissile dislocation junction

Generally, two pinning points emerge after junction forms. At a small scale, there is a high-probability that one of the pinning points escaped from the surface. Thus, a glissile junction with only one pinning point is firstly considered in this study as shown in Fig. 7a. Initially, Arm 1 is along $\boldsymbol{\zeta}_1 = [1\ -1\ 2]$, with burgers vector $\mathbf{b}_1 = [\bar{1}10]$, slip plane normal vector $\mathbf{n}_1 = (11\bar{1})$, Arm 2 is along $\boldsymbol{\zeta}_2 = [-1\ 1\ 2]$, with $\mathbf{b}_2 = [10\bar{1}]$, $\mathbf{n}_2 = (111)$, and junction segment is along $\boldsymbol{\zeta}_{jun} = [-1\ 1\ 0]$, with $\mathbf{b}_{jun} = [01\bar{1}]$, $\mathbf{n}_{jun} = (111)$.

Three kinds of strain-controlled tests are carried out. (1) Monotonic tension test is first applied to evaluate the strength of junction, which is defined as the instantaneous stress value when the pinning point disappears due to unzipping or surface annihilation; (2) Low cyclic tension strain test is second applied to examine the cyclic stability of the junction. The maximum normal strain is twice the minimum one, $\varepsilon_{max} = 2\varepsilon_{min} = 0.2\%$. (3) The third one results in stress relaxation test, i.e. the total normal strain first increases to 0.2%, and then remains constant. This test is designed to check whether the junction failure under cyclic deformation is a time dependent process.

Once the pinning point disappears due to unzipping or surface annihilation, the junction "fails" to lock the dislocations inside the sample. Hence, the attention is focused on the position of the pinning point to discuss the junction stability. Considering that the pinning point can only move along the intersection line between two slip planes $\mathbf{n}_1$ and $\mathbf{n}_2$, the distance to free surface is defined as a length x between the pinning point and free surface along the intersection line, as shown in Fig. 7a.

Fig. 8 shows the simulation result for monotonic tension test. For this considered junction, by simple calculation, the initial Peach–Koehler (PK) force on Arm 2 is along $[-1\ 1\ 0]$, and the PK force on junction segment is along $[1\ 1\ -2]$. Thus, the increasing PK force first makes dislocation Arm 2 and the junction segment meet and react with each other (see the purple dislocation snapshot in Fig. 8b). Then, dislocations gradually glide out of the crystal upon higher stress. Finally, the pinning point annihilates from the surface at 265 MPa, which is considered as the strength of the junction.

During cyclic tension test, the cyclic peak stress (140 MPa) is much lower than the strength of the junction obtained in monotonic tension. However, it can be found from Fig. 9 that the junction also gradually fails. The detailed evolution of the pinning point position is given in Fig. 9a. It can be found that after each loading cycle, the pinning point does not move back to its previous position, but shifts away from its previous position by dx. The shift direction after each strain cycle is a kind of random but the accumulated effect is that the pinning point moves toward a free surface. In addition, the general trend for the magnitude of the shift distance after each straining cycle is to increase with increasing cycle numbers. Fig. 9b shows the

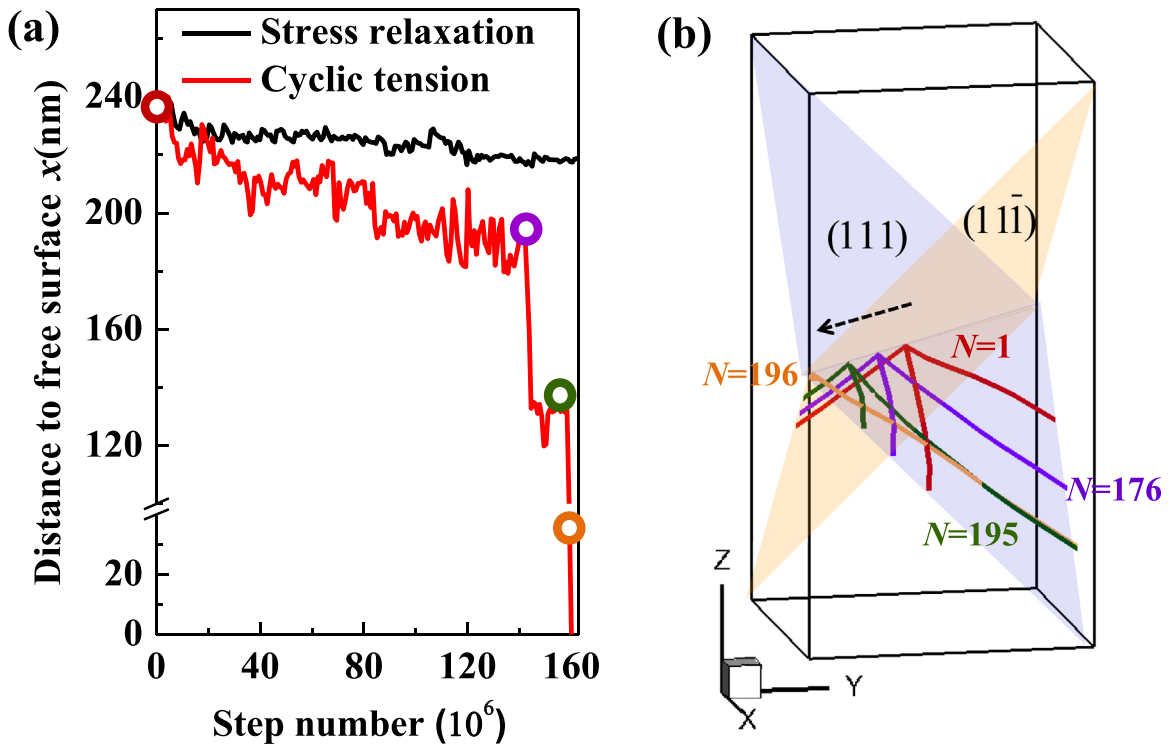

Fig. 9. (a) Evolution of distance of pinning point to free surface under cyclic tension and stress relaxation for a glissile junction. The total step number corresponds to 200 cycles; (b) snapshots of dislocation configuration corresponding to the same color marked circles in curve (a). (For interpretation of the references to color in this figure legend, the reader is referred to the web version of this article.)

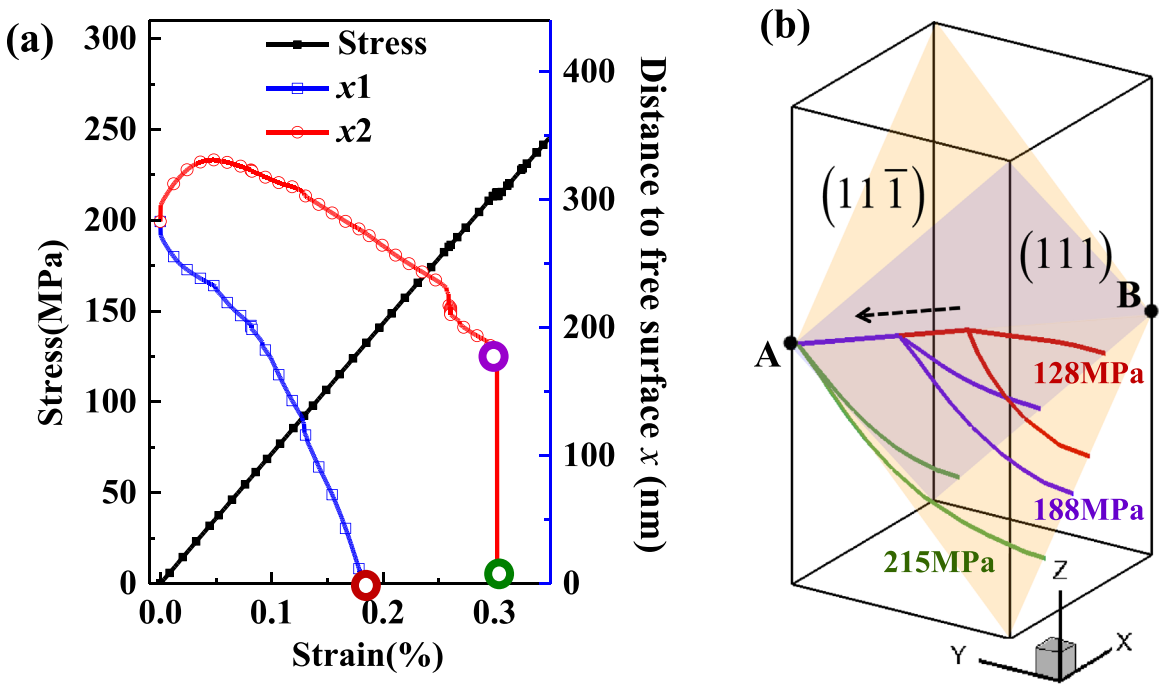

Fig. 10. (a) Evolution of stress and distance of pinning point to free surface under monotonic tension for a LC junction, $x1$ and $x2$ represent the distance for the first and second pinning point, respectively; (b) snapshots of dislocation configuration corresponding to the same color marked circles in curve (a) after the first pinning point annihilates. (For interpretation of the references to color in this figure legend, the reader is referred to the web version of this article.)

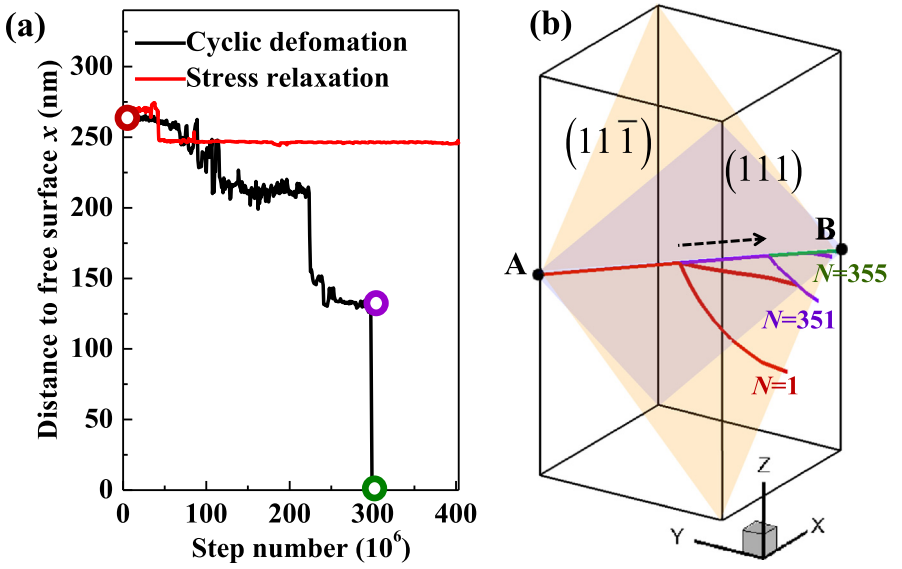

Fig. 11. (a) Evolution of distance of pinning point to free surface under cyclic tension and stress relaxation for a LC junction. The total step number corresponds to 480 cycles; (b) snapshots of dislocation configuration corresponding to the same color marked circles in curve (a).

configuration evolution of the dislocation junction that corresponds to the cycles marked with hollow circles with different colors. When the pinning point becomes close enough to the surface, the unstable dislocation junction is destroyed by fatal attraction to the free surface. At the same time, the dislocation segments escape very fast from the free surface and leave behind a nearly perfect crystal.

In contrast to test (1) and (2), the junction almost stays at a stable configuration for stress relaxation test (3), as shown in Fig. 9a. Since the total loading time for stress relaxation and cyclic deformation is the same, their totally different responses

illustrate that the cyclic effect is the key factor in triggering dislocation starvation and junction destruction instead of the time accumulation. Note that compared with the process under monotonic loading, it takes much longer time to fail the junction, because the irreversibility part of dislocation slip only occupies a small fraction of the total slip amount for each cycle, especially for such low-amplitude cyclic loading.

Similar cyclic instability process of junction failure and the cyclic enhanced mobile dislocation annihilation are also observed, when the cyclic tension loading condition is changed to the cyclic compression condition (see Appendix A).

3.2.2. Sessile dislocation junction

In light of these inspiring results for glissile junction, the sessile dislocation junction is also considered under monotonic, cyclic and relaxation loading conditions. The loading parameters are the same as those for glissile junction. Here, a LC lock is naturally formed by the interaction of two straight surface dislocation lines crossing each other at their midpoints. One dislocation line is initially along $\boldsymbol{\zeta}_1=[-1\ 1\ 0]$, with burgers vector $\mathbf{b}_1=[10\bar{1}]$, slip plane normal vector $\mathbf{n}_1=(111)$. The other one is initially along $\boldsymbol{\zeta}_2=[0\ 1\ 1]$, with $\mathbf{b}_2=[0\ 1\ 1]$, $\mathbf{n}_2=(11\bar{1})$.

The monotonic tension result is given in Fig. 10. Here, the distance to free surface is defined as a length between the pinning point and point A. It can be seen form Fig. 10b that both pinning points subsequently annihilate from the left-side surface. The junction finally fails at about 215 MPa.

The cyclic tension and stress relaxation results are shown in Fig. 11. Since the first pinning point annihilates in the first cycle, only the results for the second pinning point are given. The distance to free surface is defined as a length between pinning point and point B, because the second pinning point progressively escapes from the right-side surface (see Fig. 11b), which differs from that under monotonic tension (see Fig. 10b). The cyclic failure process for LC lock is similar to that for glissile junction. However, since the LC lock segment cannot move in crystal slip plane, an immobilized lock segment AB (see Fig. 11b) leaves along the intersection line. Moreover, during stress relaxation, the dislocation junction almost keeps stable, suggesting that the junction cyclic failure process is time insensitive.

4. Cyclic enhanced dislocation annihilation mechanism

The simulation results above clearly show that the cyclic loading can enhance the junction destruction and surface annihilation. To indicate the underlying dislocation mechanism, the different junction failure processes under monotonic loading and cyclic loading are further schematically presented in Fig. 7b and c. Under monotonic deformation, it is the relative high stress that leads to the failure of dislocation junction. The pinning point monotonously moves towards free surface upon increasing loading. Under cyclic deformation, the pinning point always glides to-and-fro between two equilibrium positions corresponding to the maximum strain $\varepsilon_{\max}$ and the minimum strain $\varepsilon_{\min}$ in one cycle as shown in Fig. 7c. The equilibrium position of pinning point is determined by minimizing the total potential energy of the entire structures (Picu and Soare, 2010). This can be simplified to solve equations to make sure the forces exerted on the pinning point by three intersecting segments to be equal to zero along the intersection line (Dupuy and Fivel, 2002). Since the external applied stress is always tension stress during deformation, its corresponding PK stress always makes dislocations glide towards a given direction, and thus makes pinning point move also towards a given direction. In contrast, the line tension force (see Fig. 9b) and the image force will assist the motion toward free surface, but opposite the returning motion. Therefore, the reverse motion in each cycle does not entirely cancel out the forward motion as shown in Fig. 7c. This irreversible movement gradually accumulates and makes the pinning point move towards surface. When the pinning point gets close enough to the free surface, the image force will play a significant role in promoting the motion towards surface. Finally, the dislocation segments glide out of the crystal. The cyclic annihilation process of mobile dislocation is also similar to the cyclic instability process of dislocation junction, as shown in Appendix A.

Accordingly, the cumulative irreversible slip plays a crucial role in dislocation self-organization and surface annihilation. Generally, the main origin of cyclic slip irreversibility includes four parts (Mughrabi, 2009): the surface annihilation, the mutual annihilation of opposite sign dislocations, cross-slip of screw dislocations and random to-and-fro glide of dislocations. All these slip irreversibility will manifest themselves in one form or another at the dislocation structure evolution. At small scales, it can favor the destruction of dislocation junctions and provide the desired conditions for surface annihilation.

5. Discussion

Based on the insight revealed by the simulation results, some discussion on how cyclic slip irreversibility contributes to critical sizes of mechanical annealing in submicron single crystals are preliminarily addressed in this section.

5.1. Dislocation density influenced by cyclic slip irreversibility

Here, the degree of cyclic slip irreversibility is implicitly characterized by dislocation density evolution equations. The theoretical investigations indicate that the change of total dislocation density $\mathrm{d}\rho$ under monotonic loading consists of four parts: dislocation multiplication due to forest dislocations $\mathrm{d}\rho_{\mathrm{mult}}$, dislocation surface annihilation $\mathrm{d}\rho_{\mathrm{surf}}$, dislocation mutual

annihilation for closely spaced dislocations of opposite sign $d\rho_{inner}$ and dislocation generation by single arm source operation $d\rho_{SAS}$ (Cui et al., 2014),

$$d\rho = d\rho_{mult} + d\rho_{surf} + d\rho_{inner} + d\rho_{SAS} \tag{1}$$

Since the low peak stress is not high enough to trigger the complete activation of single arm source, the fourth term is ignored in the following discussions. Among the first three terms on the right side of Eq. (1), the multiplication term is not fully reversible. For example, the bowing dislocations may interact with other dislocations, cross slip, or are strongly influenced by the image force induced by free surface. All these processes prevent them from returning to the original shape. Under the low-amplitude cyclic loading condition, the dislocation segments will bow out during the loading stage, leading to the increase of dislocation density. Then, during the unloading stage, the shrinkage of dislocation segments will decrease the dislocation density. Accordingly, the recovery part of dislocation multiplication during unloading stage $d\rho_{recovery-mult}$ will suppress the increase of dislocation density.

For simplicity, a dimensionless parameter k_{rm} is proposed to reflect the effect of reversible dislocation slip on the multiplication rate,

$$k_{rm} = \frac{\sum_{d\varepsilon<0} d\rho_{recovery-mult}}{\sum_{d\varepsilon>0} d\rho_{mult}} \tag{2}$$

At the same time, the dislocation surface annihilation and mutual annihilation parts are entirely irreversible, but they will be enhanced by the incomplete reversible dislocation slip as indicated by the simulation results in Section 3 and described in Section 4. Thus, the cyclic slip irreversible part will promote the decrease of dislocation density. Assuming $d\rho_{irrever-anni}$ denotes the dislocation surface and mutual annihilation enhanced by the irreversible dislocation slip, a dimensionless parameter k_{ira} is defined to reflect the effect of irreversible dislocation slip on the annihilation rate,

$$k_{ira} = \frac{\sum_{d\varepsilon>0} d\rho_{irrever-anni}}{\sum_{d\varepsilon>0} d\rho_{surf} + d\rho_{inner}} \tag{3}$$

The values of k_{rm} and k_{ira} change during deformation, and mainly depend on the dislocation configuration, cyclic number and amplitude of applied strain. During the first several cycles, the bowing dislocations have high-possibility to interact with the other dislocations, so the recoverable multiplication coefficient k_{rm} is low. However, there is higher possibility to find mobile dislocations which are attractive and tends to annihilate each other, or are close to free surface but have not glided out of the crystal yet. Therefore, the coefficient of annihilation enhanced by irreversible slip k_{ira} is high. When the cyclic number is large, relative stable dislocation configuration is formed. The recoverable multiplication coefficient k_{rm} is high. However, irreversibility mainly manifests itself through irreversible slip induced by image force and cross slip, so k_{ira} is low. As for the strain amplitude, in general, small to-and-fro dislocation displacements are more reversible than larger ones (Mughrabi, 2009). Thus, the smaller the amplitude of applied strain is, the larger the value of k_{rm} and the smaller the value of k_{ira} are. From a quantitative standpoint, it is difficult to develop a mathematical expression for these two parameters. Given the material and loading conditions, k_{rm} and k_{ira} can be estimated by fitting experimental data or simulation results.

Eq. (1) gives the dislocation density evolution law for monotonic deformation. Based on the analysis above, the unique partial reversible dislocation multiplication and irreversible slip enhanced dislocation annihilation should be taken into account to analyze the mechanical annealing phenomenon. In addition, a dimensionless parameter is introduced to approximately consider the different dislocation annihilation ability during loading and unloading stages,

$$k_u = \frac{\sum_{d\varepsilon<0} d\rho_{surf} + d\rho_{inner}}{\sum_{d\varepsilon>0} d\rho_{surf} + d\rho_{inner}} \tag{4}$$

since dislocation annihilation occurs dominantly during loading stage, k_u is less than 1. Besides, the cyclic enhanced annihilation effect is considered during the loading stage. Accordingly, the following expression for dislocation density evolution is developed to distinguish loading and unloading,

$$\rho_i = \begin{cases} \rho_{i-1} + d\rho_{mult} + (1 + k_{ira})(d\rho_{surf} + d\rho_{inner}) & (d\varepsilon > 0) \\ \rho_{i-1} - k_{rm} d\rho_{mult} + k_u(d\rho_{surf} + d\rho_{inner}) & (d\varepsilon < 0) \end{cases} \tag{5}$$

In the following, unless specified indication, the subscript i and $i-1$ denote the variables at the ith and $(i-1)$th time increment, respectively.

According to the earlier work by Gilman (1969), the multiplication term $d\rho_{mult}$ can be written as a function of breeding coefficient δ, which is defined as the inverse of the mean free path that the dislocation should move along before storage. Generally, δ is set as a function of dislocation density (Ungar et al., 2011; Zhou et al., 2011).

$$d\rho_{mult} = \rho\delta v dt, \quad \delta = f(\rho) = k_f\sqrt{\rho} \tag{6}$$

where v is dislocation velocity, k_f is a dimensionless proportionality coefficient accounting for the details of dislocation

structure (Pantleon, 2004) and loading orientations (Devincre et al., 2008).

Following Greer (2006), the dislocation surface annihilation term $d\rho_{surf}$ can be derived by assuming that the probability of dislocation escape from surface is 1/2 if a dislocation segment locates in the region within a distance vdt away from the surface. To take the slip orientation into account, Zhou et al. (2011) have derived a modified surface annihilation equation for mono-crystal of single-slip orientation,

$$d\rho_{surf} = -\rho\left(\frac{\pi(a/2 + d/2)v\ dt}{\pi ad/4}\right) = -\rho\frac{2\cos^2(\beta/2)vdt}{d} \tag{7}$$

where β is an angle between the primary slip plane normal and the axial direction of pillar. d is a diameter of pillar. $a=d/\cos\beta$, which is a major axis of the ellipse slip plane in cylindrical sample. The inner mutual annihilation term $d\rho_{inner}$ is described as a function of effective annihilation distance y (Ungar et al., 2011),

$$d\rho_{inner} = -\rho y\cdot d\varepsilon^p/(bM) \tag{8}$$

where b is burgers vector with magnitude of 0.29 nm for aluminum. y is specified as $6b$ (Cleveringa et al., 2000; Kubin et al., 1992), M is Schmid factor. Combined with the relationship between the axial plastic strain increment $d\varepsilon^p$ and the dislocation slip amount $d\varepsilon^p = M\rho bvdt$, Eq. (5) can be expressed as follows,

$$\rho_i = \begin{cases} \rho_{i-1} + (k_f\sqrt{\rho_{i-1}} - (1 + k_{ira})\dfrac{2\cos^2(\beta/2)}{d} - (1 + k_{ira})\rho_{i-1}y)\dfrac{d\varepsilon^p}{Mb} & (d\varepsilon > 0) \\ \rho_{i-1} + (-k_{rm}k_f\sqrt{\rho_{i-1}} - k_u\dfrac{2\cos^2(\beta/2)}{d} - k_u\rho_{i-1}y)\dfrac{d\varepsilon^p}{Mb} & (d\varepsilon < 0) \end{cases} \tag{9}$$

5.2. Critical size for mechanical annealing

One important issue is the critical size for mechanical annealing. For low-amplitude cyclic deformation, $d\varepsilon^p$ periodically changes sign. Therefore, the dislocation density law varies with it. If the sum of dislocation density change is negative during loading and unloading stage for each cycle, the dislocation density can gradually drop to zero within cycles. This condition can be expressed by $d\rho(d\varepsilon < 0) + d\rho(d\varepsilon > 0) < 0$. According to the simulation results in Fig. 6, the plastic deformation amount during forward loading is approximately equal to that during reverse loading in one cycle. Therefore, this condition is approximated by $d\rho/d\varepsilon^p(d\varepsilon < 0) + d\rho/d\varepsilon^p(d\varepsilon > 0) < 0$. Combining with Eq. (9), the critical size for mechanical annealing is estimated by the following relationship,

$$\begin{aligned} d_{crit\_cyclic} &= \frac{2(1 + k_{ira} + k_u)\cos^2(\beta/2)}{(1 - k_{rm})k_f\sqrt{\rho} - (1 + k_{ira} + k_u)\rho y} \\ &= \frac{2\cos^2(\beta/2)}{\sqrt{\rho}((1 - k_{rm})k_f/(1 + k_{ira} + k_u)) - \rho y} \geq \frac{2\cos^2(\beta/2)}{\sqrt{\rho} - \rho y} \end{aligned} \tag{10}$$

Only when the sample size is smaller than this critical value, the dislocation annihilation within cycles can occur. For a large sample, the crystal exhibits the bulk-like dislocation accumulation trend during continued cyclic deformation. Previous studies suggest that (Malygin, 2012; Zhou et al., 2011), the value of k_f varies from 10^{-2} to 1. At the same time, the analyses in Section 5.1 indicate that the values of k_r, k_{ira} and k_u range from 0 to 1. Therefore, $(1-k_r)\ k_f/(1+k_{ira}+k_u)$ in Eq. (10) varies from 0 to 1. The minimum value of critical diameter can be estimated according to Eq. (10). For the considered experiment cases in Section 2, the loading orientation is along $[\bar{1}11]$ direction, and the initial density of long dislocation line is $20\times10^{12}\ m^{-2}$. The critical diameter for mechanical annealing under low-amplitude cyclic loading should be larger than 300 nm. This explains why the mechanical annealing phenomenon is observed in the considered sample with cross section size $300\times500\ nm^2$, but not observed in the other experiments with larger sample size.

Similarly, the critical size for thorough mechanical annealing under monotonic deformation can also be predicted according to its dislocation density evolution equation. If $d\rho/d\varepsilon^p < 0$ and $d\varepsilon^p > 0$, the dislocation density can gradually decrease to zero during deformation. Therefore, the critical size for mechanical annealing under monotonic deformation can be estimated by $d\rho/d\varepsilon^p = 0$.

Note that for micropillar with moderate dislocation density and diameter ranging from 200 nm to 1000 nm, the operation of single arm source also contributes to the dislocation generation. If strong single arm sources form and operate continuously, the dislocation density will reach a stable value after a sharp decrease (Cui et al., 2014). Thus, the dislocation starvation state can only reach if a micropillar with initial dislocation density is lower than the stable dislocation density. Combining Eqs. (1), (6), (7) and (8), the critical condition for thorough mechanical annealing under monotonic deformation can be expressed as follows,

$$\frac{d\rho}{d\varepsilon^p} = \frac{1}{bM}\left(\frac{1}{2\bar{\lambda}} - \frac{2\cos^2(\beta/2)}{d} + k_f\sqrt{\rho} - y\rho\right) = 0 \tag{11}$$

where $\bar{\lambda}$ is a length of the statistic average effective single arm sources, which can be expressed as function of dislocation density and pillar diameter (Jennings et al., 2012; Parthasarathy et al., 2007; Zhou and LeSar, 2012). The critical diameter for through dislocation annihilation can be estimated as follows,

$$d_{\text{crit\_monotonic}} = \frac{2\cos^2(\beta/2)}{\frac{1}{2\bar{\lambda}(d_{\text{crit\_monotonic}},\rho)} + k_f\sqrt{\rho} - \rho y} < d_{\text{crit\_cyclic}} \tag{12}$$

Comparing Eq. (12) with Eq. (10), it is easy to derive that the thorough mechanical annealing can take place in larger size under cyclic deformation than that under monotonic deformation. If k_f is set to 10^{-2} (Malygin, 2012) and monotonic loading orientation is along [001], for the FIB fabricated micropillar with initial dislocation density $10^{14}\,\text{m}^{-2}$, the critical pillar diameter for mechanical annealing is calculated as about 130 nm, according to Eq. (12). This is close to the sample size (the top diameter of the pillar is 160 nm) where dislocation starvation is observed via in situ TEM under monotonic compression test (Shan et al., 2008). It also explains why dislocation starvation is rarely observed in larger pillar under monotonic loading.

To realize mechanical annealing by imposing external loading, the surface annihilation plays a very important role. Thus, both phenomena are apt to occur in smaller size, which means more pronounced image force, shorter mean free path and larger specific surface area for surface annihilation. During monotonic loading, the high-stress destructs the dislocation junction and increases the probability of making the dislocations move to the near surface region. During low-amplitude cyclic loading, both dislocation junction failure and surface annihilation are enhanced by cumulative irreversible slip. The difference on dislocation mechanism makes mechanical annealing under cyclic loading can occur in larger sample under lower applied stress and producing smaller shape change.

6. Conclusions

Experimental and simulation results indicate that cyclic loading with low-stress amplitude can drive the dislocations out of the submicron single crystal without seriously change the structure shape. It is found that during the first several cycles, mobile dislocations glide out of the crystal and weak junctions destruct. During the subsequent cycles, dislocation density increases during loading stage and decreases more significantly during unloading stage, causing a gradual decline of dislocation density within cycles. Dislocation junction can be gradually destroyed during cyclic deformation, even when the cyclic peak stress is much lower than that required to break them under monotonic deformation. The cumulative irreversible slip is found to be the key factor of promoting junction destruction and dislocation annihilation at free surface under low-amplitude cyclic loading condition. By considering this cyclic slip irreversibility, the preliminary discussion is further given to explain why a critical size exists for mechanical annealing under cyclic loading and monotonic loading mode.

It is discovered that the mechanical annealing under low-stress cyclic loading condition is induced by the more significant surface annihilation enhanced by cyclic irreversible slip, and the weaker dislocation multiplication induced by the reversible part and relative low-stress. Thus, compared with monotonic deformation, mechanical annealing can occur in larger size, under lower stress and with much smaller shape change. This low-stress cyclic deformation method offers a potential route to form and manufacture pristine submicron devices with high-strength. The current finding also sheds the light on controlling the dislocation evolution history by designing external loading.

Acknowledgments

This work is supported by the National Natural Science Foundation of China under Grant no. 11132006, 11302115 and 51401159. The authors are grateful to Professor Z.W. Shan from Xi'an Jiaotong University in illuminating discussions. The authors would like to thank and appreciate the reviewers for their constructive comments and suggestions.

Appendix A. Cyclic instability of dislocation junction and mobile dislocation

In Section 3.2.1, the cyclic instability of a glissile dislocation junction is discussed. To further show the generality of the revealed process and exclude the special case that dislocation arm 2 meets the junction under monotonic loading, the compression loading is applied instead of the tension loading.

During uniaxial compression test, as shown in Fig. A1, the pinning point directly annihilates from free surface without the interaction between dislocation junction and arms. The strength of the junction under uniaxial compression is about 153 MPa. In the low cyclic compression strain test, the maximum normal strain is also twice the minimum one, $\varepsilon_{\max}=2\varepsilon_{\min}=-0.2\%$. The cyclic peak stress is about 140 MPa, which is close to the junction strength value. Thus, the pinning point disappears in the second cycle. During the subsequent cycles, the mobile dislocation gradually annihilates from free surface with the aid of incomplete reversible slip, as shown in Fig. A2. If lower cyclic compression strain test is considered with $\varepsilon_{\max}=2\varepsilon_{\min}=-0.156\%$, the cyclic peak stress is about 112 MPa, the pinning point can only annihilate from

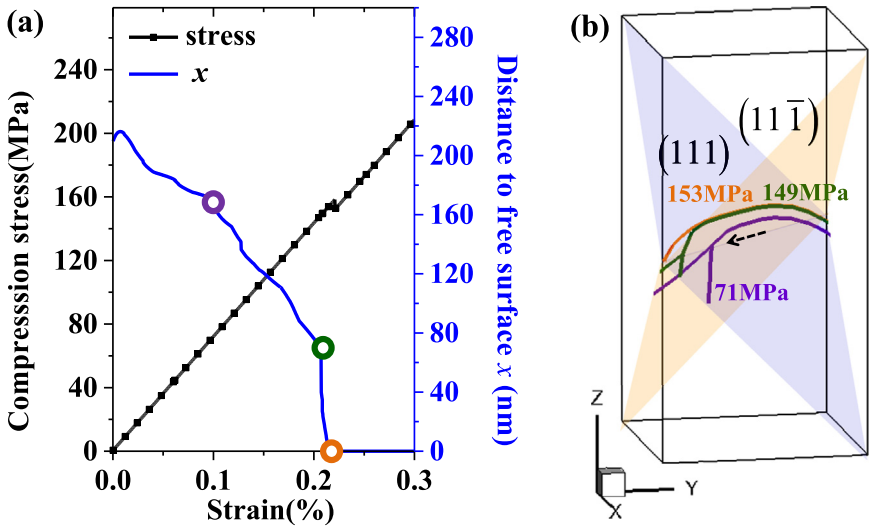

Fig. A1. (a) Evolution of stress and distance of pinning point to free surface versus applied strain under monotonic compression for a glissile junction; (b) snapshots of dislocation configuration corresponding to the same color marked circles in the curve.

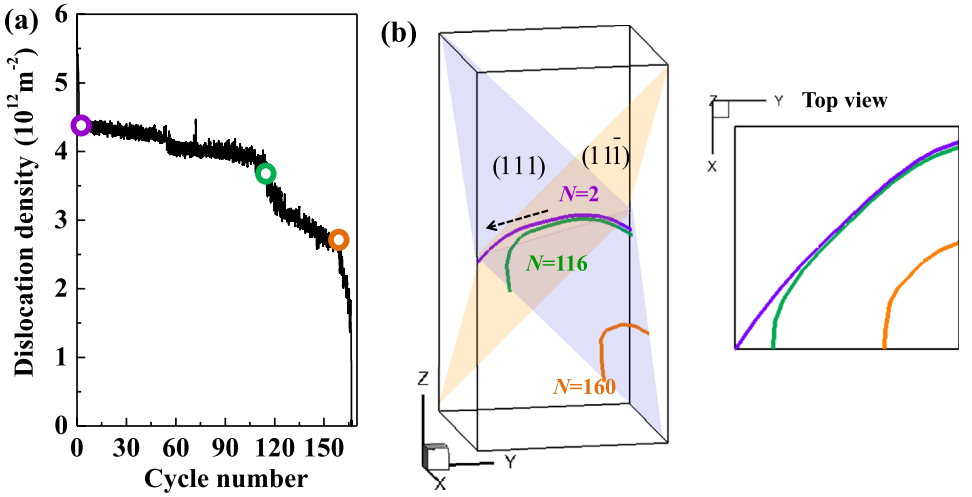

Fig. A2. (a) Evolution of dislocation density under cyclic compression for a glissile junction. Cyclic peak stress is about 140 MPa; (b) snapshots of dislocation configuration corresponding to the same color marked circles in curve (a).

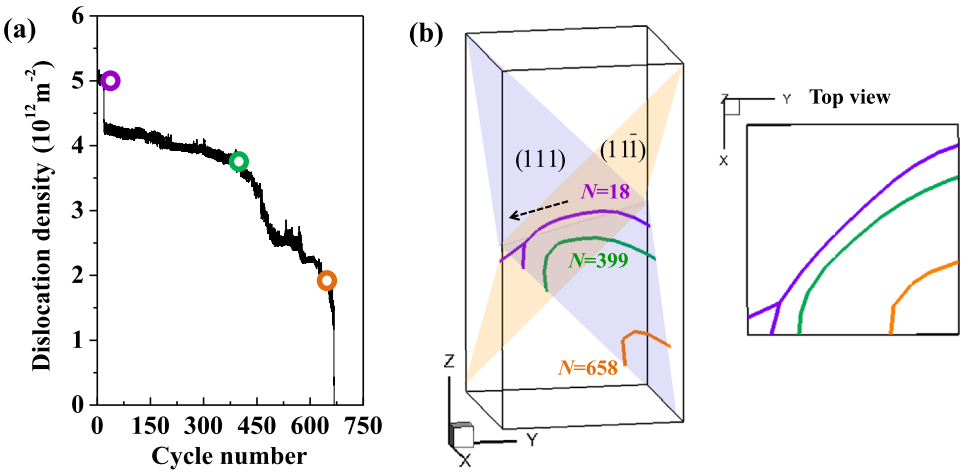

Fig. A3. (a) Evolution of dislocation density under cyclic compression for a glissile junction. Cyclic peak stress is about 112 MPa; (b) snapshots of dislocation configuration corresponding to the same color marked circles in curve (a).

free surface after 18 cycles as shown in Fig. A3. The subsequent dislocation annihilation process is similar to that shown in Fig. A2. This case not only verifies the cyclic instability of dislocation junction, but also clearly illustrates how cyclic stress contributes to the gradual annihilation of mobile dislocation.

References

Aifantis, E.C., 1987. The physics of plastic deformation. Int. J. Plast. 3, 211–247.
Alpay, S.P., Misirlioglu, I.B., Nagarajan, V., Ramesh, R., 2004. Can interface dislocations degrade ferroelectric properties? Appl. Phys. Lett. 85, 2044–2046.
Bei, H., Shim, S., Pharr, G.M., George, E.P., 2008. Effects of pre-strain on the compressive stress–strain response of Mo-alloy single-crystal micropillars. Acta Mater. 56, 4762–4770.
Cleveringa, H.H.M., Van der Giessen, E., Needleman, A., 2000. A discrete dislocation analysis of mode I crack growth. J. Mech. Phys. Solids 48, 1133–1157.
Csikor, F.F., Motz, C., Weygand, D., Zaiser, M., Zapperi, S., 2007. Dislocation avalanches, strain bursts, and the problem of plastic forming at the micrometer scale. Science 318, 251–254.
Cui, Y.N., Liu, Z.L., Zhuang, Z., 2015a. Theoretical and numerical investigations on confined plasticity in micropillars. J. Mech. Phys. Solids 76, 127–143.
Cui, Y.N., Lin, P., Liu, Z.L., Zhuang, Z., 2014. Theoretical and numerical investigations of single arm dislocation source controlled plastic flow in FCC micropillars. Int. J. Plast. 55, 279–292.
Cui, Y.N., Liu, Z.L., Zhuang, Z., 2015b. Quantitative investigations on dislocation based discrete–continuous model of crystal plasticity at submicron scale. Int. J. Plast. 69, 54–72.
Déprés, C., Fivel, M., Tabourot, L., 2008. A dislocation-based model for low-amplitude fatigue behaviour of face-centred cubic single crystals. Scr. Mater. 58, 1086–1089.
Devincre, B., 1996. Meso-scale simulation of the dislocation dynamics. NATO ASI Ser. E 308, 309–324.
Devincre, B., Hoc, T., Kubin, L., 2008. Dislocation mean free paths and strain hardening of crystals. Science 320, 1745–1748.
Dupuy, L., Fivel, M.C., 2002. A study of dislocation junctions in FCC metals by an orientation dependent line tension model. Acta Mater. 50, 4873–4885.
El-Awady, J.A., 2015. Unravelling the physics of size-dependent dislocation-mediated plasticity. Nat. Commun. 6, 5926.
El-Awady, J.A., Wen, M., Ghoniem, N.M., 2009. The role of the weakest-link mechanism in controlling the plasticity of micropillars. J. Mech. Phys. Solids 57, 32–50.
Espinosa, H.D., Panico, M., Berbenni, S., Schwarz, K.W., 2006. Discrete dislocation dynamics simulations to interpret plasticity size and surface effects in freestanding FCC thin films. Int. J. Plast. 22, 2091–2117.
Franciosi, P., Zaoui, A., 1982. Multislip tests on copper crystals: a junctions hardening effect. Acta Metall. 30, 2141–2151.
Gao, Y., Liu, Z.L., You, X.C., Zhuang, Z., 2010. A hybrid multiscale computational framework of crystal plasticity at submicron scales. Comput. Mater. Sci. 49, 672–681.
Gilman, J.J., 1969. Micromechanics of Flow in Solids. McGraw-Hill, New York.
Greer, J.R., 2006. Bridging the gap between computational and experimental length scales: a review on nano-scale plasticity. Rev. Adv. Mater. Sci. 13, 59–70.
Greer, J.R., Nix, W.D., 2006. Nanoscale gold pillars strengthened through dislocation starvation. Phys. Rev. B 73, 245410.
Groh, S., Zbib, H.M., 2009. Advances in discrete dislocations dynamics and multiscale modeling. J. Eng. Mater. Technol. 131, 041209.
Hussein, A.M., Rao, S.I., Uchic, M.D., Dimiduk, D.M., El-Awady, J.A., 2015. Microstructurally based cross-slip mechanisms and their effects on dislocation microstructure evolution in fcc crystals. Acta Mater. 85, 180–190.
Jennings, A.T., Gross, C., Greer, F., Aitken, Z.H., Lee, S.-W., Weinberger, C.R., Greer, J.R., 2012. Higher compressive strengths and the Bauschinger effect in conformally passivated copper nanopillars. Acta Mater. 60, 3444–3455.
Kubin, L.P., Canova, G., Condat, M., Devincre, B., Pontikis, V., Bréchet, Y., 1992. Dislocation microstructures and plastic flow: a 3D simulation. Solid State Phenom. 23, 455–472.
Lee, S.-W., Jennings, A.T., Greer, J.R., 2013. Emergence of enhanced strengths and Bauschinger effect in conformally passivated copper nanopillars as revealed by dislocation dynamics. Acta Mater. 61, 1872–1885.
Liu, Z.L., Liu, X.M., Zhuang, Z., You, X.C., 2009. A multi-scale computational model of crystal plasticity at submicron-to-nanometer scales. Int. J. Plast. 25, 1436–1455.
Malygin, G.A., 2012. Influence of the transverse size of samples with micro-and nano-grained structures on the yield and flow stresses. Phys. Solid State 54, 559–567.
Motz, C., Weygand, D., Senger, J., Gumbsch, P., 2008. Micro-bending tests: a comparison between three-dimensional discrete dislocation dynamics simulations and experiments. Acta Mater. 56, 1942–1955.
Motz, C., Weygand, D., Senger, J., Gumbsch, P., 2009. Initial dislocation structures in 3-D discrete dislocation dynamics and their influence on microscale plasticity. Acta Mater. 57, 1744–1754.
Mughrabi, H., 2009. Cyclic slip irreversibilities and the evolution of fatigue damage. Metall. Mater. Trans. A 40, 1257–1279.
Pantleon, W., 2004. Stage IV work-hardening related to disorientations in dislocation structures. Mater. Sci. Eng. A 387, 257–261.
Parthasarathy, T.A., Rao, S.I., Dimiduk, D.M., Uchic, M.D., Trinkle, D.R., 2007. Contribution to size effect of yield strength from the stochastics of dislocation source lengths in finite samples. Scr. Mater. 56, 313–316.
Picu, R.C., Soare, M.A., 2010. Asymmetric dislocation junctions exhibit a broad range of strengths. Scr. Mater. 62, 508–511.
Rajagopalan, J., Han, J.H., Saif, M.T.A., 2007. Plastic deformation recovery in freestanding nanocrystalline aluminum and gold thin films. Science 315, 1831–1834.
Rao, S.I., Dimiduk, D.M., Parthasarathy, T.A., Uchic, M.D., Tang, M., Woodward, C., 2008. Athermal mechanisms of size-dependent crystal flow gleaned from three-dimensional discrete dislocation simulations. Acta Mater. 56, 3245–3259.
Rodney, D., Phillips, R., 1999. Structure and strength of dislocation junctions: an atomic level analysis. Phys. Rev. Lett. 82, 1704–1707.
Shan, Z.W., Mishra, R.K., Asif, S.A.S., Warren, O.L., Minor, A.M., 2008. Mechanical annealing and source-limited deformation in submicrometre-diameter Ni crystals. Nat. Mater. 7, 115–119.
Uchic, M.D., Shade, P.A., Dimiduk, D.M., 2009. Plasticity of micrometer-scale single crystals in compression. Annu. Rev. Mater. Res. 39, 361–386.
Ungar, T., Li, L., Tichy, G., Pantleon, W., Choo, H., Liaw, P.K., 2011. Work softening in nanocrystalline materials induced by dislocation annihilation. Scr. Mater. 64, 876–879.
Wang, Z.J., Li, Q.J., Cui, Y.N., Liu, Z.L., Ma, E., Li, J., Sun, J., Zhuang, Z., Dao, M., Shan, Z.W., Suresh, S., 2015. Cyclic deformation leads to defect healing and strengthening of small-volume metal single crystals. PNAS 112 (44), 13502–13507.
Wang, Z.J., Li, Q.J., Shan, Z.W., Li, J., Sun, J., Ma, E., 2012. Sample size effects on the large strain bursts in submicron aluminum pillars. Appl. Phys. Lett. 100, 071906.
Watling, J.R., Paul, D.J., 2011. A study of the impact of dislocations on the thermoelectric properties of quantum wells in the Si/SiGe materials system. J. Appl. Phys. 110, 114508.
Zhang, G.P., Volkert, C.A., Schwaiger, R., Wellner, P., Arzt, E., Kraft, O., 2006. Length-scale-controlled fatigue mechanisms in thin copper films. Acta Mater. 54, 3127–3139.
Zhou, C., Beyerlein, I.J., LeSar, R., 2011. Plastic deformation mechanisms of fcc single crystals at small scales. Acta Mater. 59, 7673–7682.
Zhou, C., LeSar, R., 2012. Dislocation dynamics simulations of plasticity in polycrystalline thin films. Int. J. Plast. 30, 185–201.